Electronic Supplementary Material (ESI) for Nanoscale.
This journal is © The Royal Society of Chemistry 2021

Supplementary Material

Symbiotic Assembly of Peptide Nano-Mosaics at Solid Interfaces

Tyler D. Jorgenson, Hadi M. Zareie, Mehmet Sarikaya, & René M. Overney*

* Email: roverney@uw.edu

Supplementary Notes

Note S1: Derivation of Single Phase 2D Classical Nucleation Rate

In classical nucleation theory, the nucleation rate of a crystal is proportional to the Boltzmann probability that monomers overcome an energetic nucleation barrier, Δg_n, and form cluster of critical radii.[1, 2]

$$\frac{dn}{dt} = A \exp\left(\frac{\Delta g_n}{kT}\right) \quad (S1)$$

For 2D nucleation of circular monomers, the system the total free energy is the sum of the free energy of the bulk crystal, Δg_b, and the free energy of the crystal interface, Δg_s, as follows:

$$\Delta g_{tot} = \Delta g_s + \Delta g_b = 2\pi r\lambda - \frac{\pi r^2}{A_m}\Delta\mu \quad (S2)$$

Where r is the radius of the nuclei, λ is the line-tension of the crystal-substrate interface, A_m is the area per monomer, and $\Delta\mu$ is the chemical potential difference between the monomer and the crystal phase. The critical radius occurs, r_c, occurs when the gradient of Δg_{tot} is 0.

$$0 = \frac{dg_{tot}}{dr} = 2\pi\lambda - \frac{2\pi r_c}{A_m}\Delta\mu$$

$$r_c = \frac{\lambda A_m}{\Delta\mu} \quad (S3)$$

The free energy barrier associated with forming a nucleus of critical radius, Δg_n, is thus

$$\Delta g_n = 2\pi\frac{\lambda A_m}{\Delta\mu}\lambda - \frac{\pi\left(\frac{\lambda A_m}{\Delta\mu}\right)^2}{A_m}\Delta\mu = \frac{\pi A_m\lambda^2}{\Delta\mu} \quad (S4)$$

The chemical potential, $\Delta\mu$, is most generically defined as $\Delta\mu = kTln(\alpha)$, where k is the Boltzmann constant, T is the temperature in Kelvin, and α is the activity of the system. For practical purposes it is beneficial to represent α in terms of an experimental observable in relation to a reference condition scaled by an activity coefficient, γ, that captures non-ideality. Herein, we use the peptide concentration, C, in reference to an equilibrium concentration, C_e, that denotes the concentration at which a critical nucleus will neither grow nor dissolve. Moreover, for we assume $\gamma = 1$ for single phase nucleation, i.e.,

$$\Delta\mu = kTln\left(\gamma\frac{C}{C_e}\right) \cong kTln\left(\frac{C}{C_e}\right) \xrightarrow[C/C_e \ll 1]{} kT\left(\frac{C}{C_e} - 1\right) \text{ (S5)}$$

for low concentrations. Combining equations S1, S4 and S5, the nucleation rate is

$$\frac{dn}{dt} = A \exp\left(\frac{\pi A_m\lambda^2}{(kT)^2\left(\frac{C}{C_e} - 1\right)}\right) \quad (S6)$$

Note S2: Empirical Derivation of Symbiotic Binary Assembly

The pre-exponential factor in classical nucleation theory for a single phase is,[2]

$$A_{single} = ZjN_s \quad (S7)$$

where Z is the Zeldovich factor that accounts for the sticking probability of a molecule onto the critical nuclei, j is the molecular attachment rate, and N_s is the density of nucleation sites. As the same amount of graphite is available in both the single-phase and binary assembly systems, N_s is a constant. Using classical kinetic arguments, Zj can be defined as,

$$Zj = \frac{2D}{l^2} \quad (S8)$$

where D is the diffusion coefficient of the nuclei and l is the mean free path of the monomer. We assume that D is constant for both the single-phase and binary systems. The square of the mean free path, l^2, represents the amount of area the monomer can search before a collision, for instance, with a nucleus. In the binary system, we anticipate l^2 decreases with decreasing molar fraction, ζ, as the dominate peptide phase will block surface sites. Moreover, we hypothesis that the preferential growth direction translates to directional diffusion and an increase in a monomer's collision probability with its' respective phase's nuclei. Mathematically we may decrease l^2 by multiplying by ζ. Thus, the binary pre-exponential factor is

$$A_{binary} = \frac{2D}{\zeta l^2} N_s = \frac{A_{single}}{\zeta} \quad (S9)$$

This decrease in available surface area will increase the local density of the peptide monomer with smaller ζ. Since in 2D the "concentration" is the local surface coverage of peptides, this increase in local density will artificially decrease the observed C_e we attribute to the system. We can represent this increase in activity with decreasing molar fraction by defining $\gamma = {}^{1}/_{\zeta}$, and thus,

$$\Delta\mu = kTln\left(\gamma\frac{C}{C_e}\right) = kTln\left(\frac{1}{\zeta}\frac{C}{C_e}\right) = kT\left(\frac{C}{C_e} - \zeta\right) \quad (S10)$$

Using this modified form of the chemical potential and supersaturation, the free energy barrier for critical nuclei in the binary system is:

$$\Delta g_{n,binary} = \frac{\pi A_m \lambda^2}{kT\left(\frac{C}{C_e} - \zeta\right)} \quad (S11)$$

As both the Δg_b and A_{binary} diverge for very small ζ, we must further modify equation S11 to ensure that the nucleation rate approaches zero as $\zeta \rightarrow 0$. This can be accomplished by scaling Δg_s via the line-tension, i.e., λ/ζ, so that a nucleus cannot form at small ζ. The final binary nucleation free-energy barrier is therefore,

$$\Delta g_{n,binary} = \frac{\pi A_m \left({}^{\lambda}/_{\zeta}\right)^2}{kT\left(\frac{C}{C_e} - \zeta\right)} = \frac{\pi A_m \lambda^2}{kT\zeta^2\left(\frac{C}{C_e} - \zeta\right)} \quad (S12)$$

Plugging equations S9 and S12 into S1 and accounting for multiple phases yields the nucleation rate for a symbiotic assembly,

$$\frac{dn}{dt} = \sum_i \frac{A_i}{\zeta_i} \exp\left(-\frac{\pi A_{m,i}{\lambda_i}^2}{(kT)^2{\zeta_i}^2\left(\frac{C}{C_{e,i}} - \zeta_i\right)}\right) = \sum_i \frac{A_i}{\zeta_i} \exp\left(-\frac{B_i}{{\zeta_i}^2\left(\frac{C}{C_{e,i}} - \zeta_i\right)}\right)$$

where i is the index for the constituent phase, and B is the dimensionless factor combining the energetic and geometric factors as defined for the single-phase system.

Note S3: Relationship between Nucleation & Grain Area

As the presented data is a snapshot of the equilibrium assembly after two hour incubation, the approximate growth rate of the peptide assembly is estimated by dividing the average area per grain by the incubation time, $u = \frac{<area>}{2\ hours}$.

However, as the total graphite surface area is finite, at high concentrations the apparent growth rate, u, plateaus since the surface saturates within the 2-hour incubation. The data cannot distinguish between rates for concentrations above this plateau (i.e., at 2.5 μM the surface may saturate in 30 minutes while at 1.5 μM the surface may saturate in 1 hour). The true growth rate would likely have a linear relationship with increasing concentration as demonstrated by the lower concentration range.

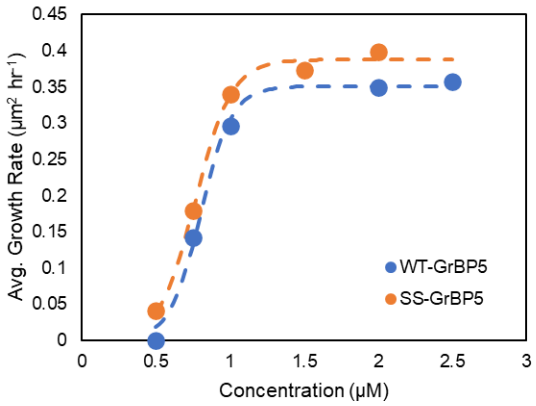

Nonetheless, at concentrations above 1 μM, the saturation of the surface provides a linear relationship between the average grain area and the nucleation rate for all molar fractions.

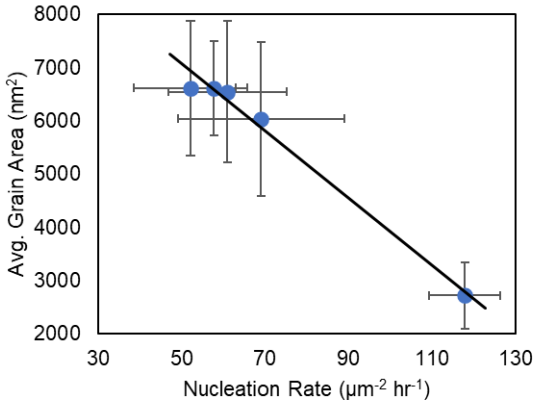

$$A_{grain} = -(63.0 \pm 4.4)\left[\frac{dn}{dt}\right] + (10212 \pm 332)$$

This linear relationship is used to translate Eqn. 3 in the manuscript to predict the binary system grain area.

Supplementary Figures

Figure S1: AFM Structural Analysis Technique

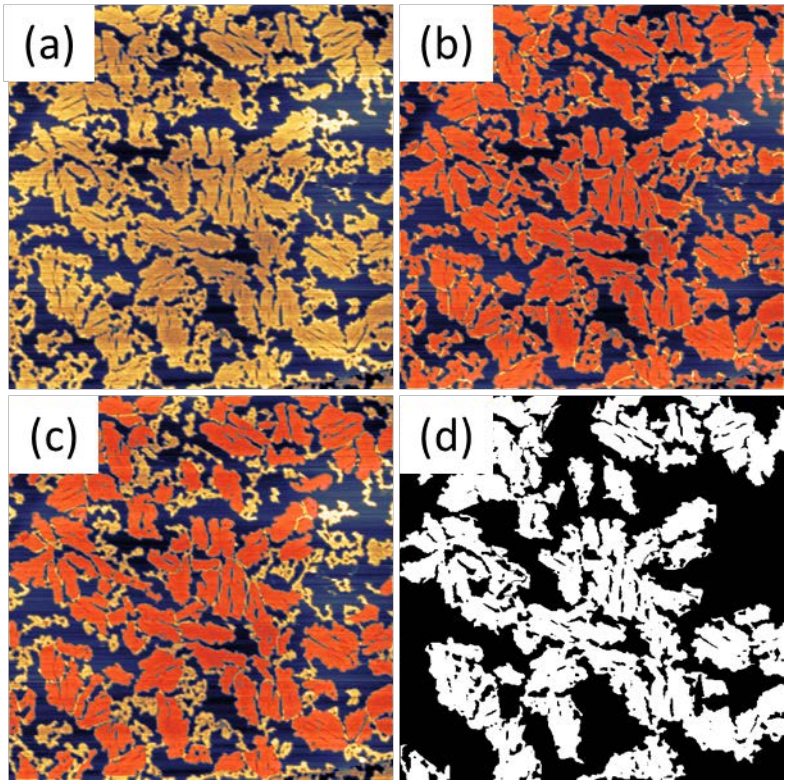

Figure S1. (a) AFM images were processed using the Gwyddion software package.[3] The images are flattened and cropped to remove graphite step edges or other defects that complicate further processing. Images sizes analyzed were always 1 μm × 1 μm. Phase or amplitude images may be used if defects cannot be cropped from the height image. (b) A mask is applied to flattened image based on height, phase, or amplitude (depending on type of image) so that the peptide is clearly distinguished from the underlying graphite surface. Manual editing of the mask was performed to remove erroneously masked graphite and separate amorphous from long-range ordered phases, and different long-range ordered grains from each other when the computer was unable to automatically do so. The mask is then filtered by a variety of grain parameters depending on the quality of the image. In part (c) the mask is filtered by grain size. This was often the most effective at separating the ordered and amorphous regions. The final edited mask was then analyzed for ordered grain size and number of ordered grains. (d) The mask was then extracted, binarized, and fast-Fourier transformed (FFT) to enhance and analyze geometric features created by the long-range ordered domains. Angles within the FFTs were manually analyzed.

Figure S2: Atomic Resolution Images of Graphite Lattice

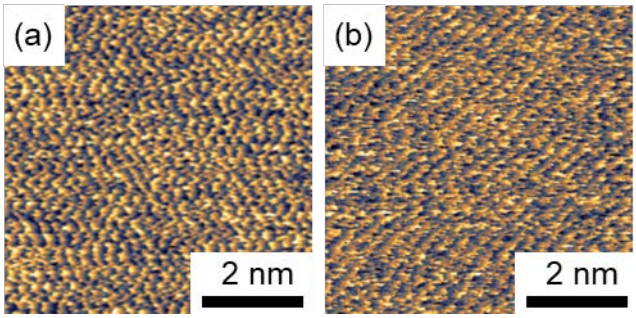

Figure S2. Contact mode SFM images of the underlying graphite lattice for (a) WT-GrBP5 and (b) SS-GrBP5. Images were processed using a plane fit and mean scan line alignment. The FFT filtering of the above HOPG lattices are displayed in Figure 4 of the main text.

Figure S3: FFT Comparison of Assembly and Lattice Angle Relationship

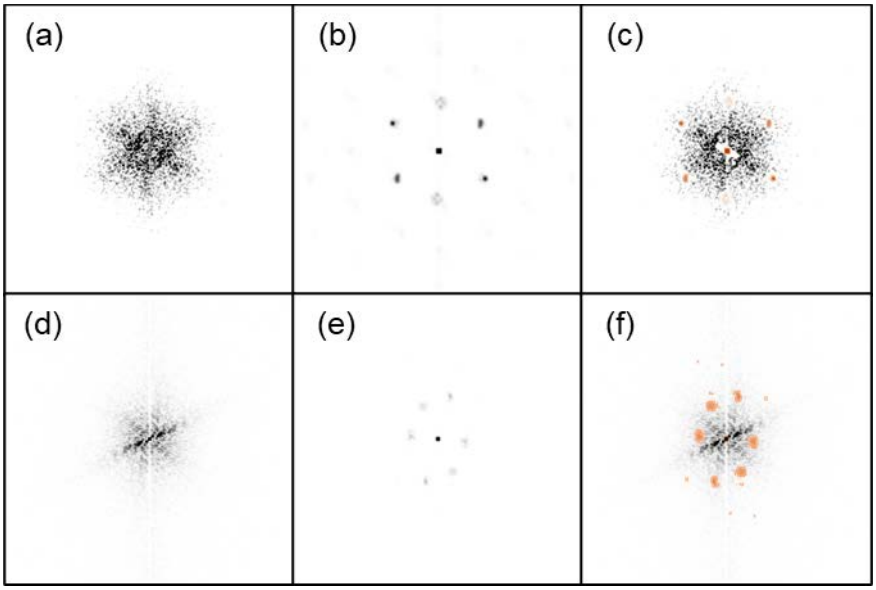

Figure S3. The fast Fourier transfrom (FFT) of the (a) WT-GrBP5 assembly, and the (b) filtered graphite FFT when superimposed (c) reveal that the assembly direction and graphite zig-zag lattice direction are nearly indentical. The same comparsion for SS-GrBP5 (d-f) show that there is a clear offset between the peptide assembly direction and the graphite zig-zag lattice direction. The filltered graphite FFTs are false colored orange in (c, f). (b) and (e) results from the backtransfrom of filtered graphite lattices presented in Figure 4 of the main text. The un-filtered graphite lattices are presented in Figure S2. This filtering process allowed for clearer comparisons between the assembly directions and the lattice directions via overlaying.

Supplementary Tables

Table S1: WT-GrBP5/HOPG Angle Relationship

	Armchair Direction		WT Assembly Direction		Orientation Relationship	
Angle	AVG*	STD	AVG*	STD		
1	33.9	2.3	30.5	3.4	-3.4	5.7
2	88.0	1.3	93.1	5.1	5.1	6.4
3	151.8	7.6	151.7	2.6	-0.1	10.2
					AVG	**STD**
					1	**7**

*Angle relative to the x-axis of the SFM image.

Table S2: SS-GrBP5/HOPG Angle Relationship

	Armchair Direction		SS Assembly Direction		Orientation Relationship	
Angle*	AVG**	STD	AVG**	STD		
1	43.2	1.7	20.5	4.4	22.7	6.1
2	162.5	3.7	141.5	2.0	21.0	5.7
					AVG	**STD**
					22	**6**

* On average only 2 angles visible in HOPG lattice image
Outlier with all 3 shown in Figure S2.
**Angle relative to the x-axis of the SFM images.

Supplementary References

1. J. J. De Yoreo and P. G. Vekilov, *Reviews in mineralogy and geochemistry*, 2003, **54**, 57-93.
2. R. P. Sear, *Journal of Physics: Condensed Matter*, 2007, **19**, 033101.
3. D. Nečas and P. Klapetek, *Open Physics*, 2012, **10**, 181-188.